Available online at www.sciencedirect.com
ScienceDirect
Atmospheric Environment 40 (2006) 7668–7685
ATMOSPHERIC ENVIRONMENT
www.elsevier.com/locate/atmosenv

Estimating fugitive dust emission rates using an environmental boundary layer wind tunnel

Jason A. Roney[a,*], Bruce R. White[b]

[a]Department of Mechanical and Aerospace Engineering, University of Colorado, 1420 Austin Bluffs Parkway, Colorado Springs, CO 80918, USA
[b]Department of Mechanical and Aeronautical Engineering, One Shields Avenue, University of California, Davis, CA 95616, USA

Received 17 February 2006; received in revised form 15 July 2006; accepted 16 August 2006

Abstract

Emissions from fugitive dust due to erosion of "natural" wind-blown surfaces are an increasingly important part of PM_{10} (particulate matter with sizes of 10 μm aerodynamic diameter) emission inventories. These inventories are particularly important to State Implementation Plans (SIP), the plan required for each state to file with the Federal government indicating how they will comply with the Federal Clean Air Act (FCAA). However, techniques for determining the fugitive dust contribution to over all PM_{10} emissions are still in their developmental stages. In the past, the methods have included field monitoring stations, specialized field studies and field wind-tunnel studies. The measurements made in this paper allow for systematic determination of PM_{10} emission rates through the use of an environmental boundary layer wind tunnel in the laboratory. Near surface steady-state concentration profiles and velocity profiles are obtained in order to use a control volume approach to estimate emission rates. This methodology is applied to soils retrieved from the nation's single largest PM_{10} source, Owens (dry) Lake in California, to estimate emission rates during active storm periods. The estimated emission rates are comparable to those obtained from field studies and lend to the validity of this method for determining fugitive dust emission rates.

Keywords: Particulate matter; Fugitive dust; Emission rates; Wind tunnel; Aerosols

1. Introduction

1.1. Overview of methodology

The primary goal of the research presented in this paper is to describe a novel methodology for determining fugitive dust emission rates using an environmental boundary layer wind tunnel in the laboratory. These measurements have not been previously made in the manner described in this paper and allow for systematic determination of emission rates that can be used in atmospheric models. A case study involving Owens (dry) Lake soils is used to exhibit the methodology. The effect of surface variability on dust entrainment is imperative in predicting concentration levels in the atmosphere. Thus, this paper may prove beneficial at other sites around the world where wind-blown

*Corresponding author. Tel.: +1 719 262 3573; fax: +1 719 262 3042.
E-mail address: jroney@eas.uccs.edu (J.A. Roney).

1352-2310/$ - see front matter © 2006 Elsevier Ltd. All rights reserved.
doi:10.1016/j.atmosenv.2006.08.015

particulate loadings need to be estimated to address environmental impacts to air quality. The present wind-tunnel simulation is not meant to be an exact simulation of all the meteorological conditions at Owens (dry) Lake or any site, but it is meant to isolate the effect of wind-erosion on dust entrainment at the surface-air interface. Through wind erosion analysis of four soils in a laboratory wind tunnel, quantification of the emission rates of dust, specifically, PM_{10} at Owens (dry) Lake are estimated using a novel approach.

A comprehensive discussion of the PM_{10} problem at Owens (dry) Lake in California and its origin is presented in our previous paper (Roney and White, 2004). Despite recent control strategies, Owens (dry) Lake is still the largest stationary PM_{10} source in the USA due to actively blowing soils which produce fugitive dust. Due to the need for dust storm mitigation at Owens (dry) Lake, the University of California at Davis became active in many of the research projects (White and Cho, 1994; Cahill et al., 1996; Kim et al., 2000; White and Roney, 2000; Roney and White, 2004) aimed at controlling the storms.

1.2. Emission rates and dust suspension

PM_{10} emission rates at sites with wind erosion are related to dust suspension. The emission rate is defined as the amount of mass suspended per unit area of surface soil per unit time. In describing suspended particles, Bagnold (1941) differentiates between "dust" and "sand": "We can thus define the lower limit of size of sand grains, without reference to their shape or material, as that at which the terminal velocity of fall becomes less than the upward eddy current within the average of the surface wind". Typically, the aerodynamic diameter at this limit is estimated at 50 μm; dust $<50\,\mu m$, and sand $>50\,\mu m$ (Lancaster and Nickling, 1994). In addition, long-term suspension of dust is estimated for diameters $<20\,\mu m$ (Pye, 1987); thus, PM_{10} has the potential for long-term suspension.

Suspension and production of dust occurs through two mechanisms; abrasion and through the direct action of the wind on the surface. Abrasion can occur through saltation (impact by sand-sized particles hopping along the surface) while wind forces cause both wind shear and turbulent shear (Braaten et al., 1993) that may suspend particles. Once in suspension, dust is transported by two means; horizontal advection, and turbulent diffusion. Both suspension and transport properties are important when estimating the emission rate of a given surface. Dust may originate from an upwind source not related to the surface (transport) or be entrained or transported locally from the surface (turbulent diffusion and advection). A true estimation of the emission rate of a surface must involve a subtraction of the non-related advection component. The upwind advection component is known for the wind-tunnel study presented in this paper, thus, a better approximation for the emission rate is made using the control volume approach for a specific soil.

To exemplify this last point, consider a typical vertical dust flux calculated with a field tower as presented in numerous studies (Gillette et al., 1972; Gillette and Goodwin, 1974; Gillette and Walker, 1977; Cahill et al., 1996; Gillette et al., 1997a; Niemeyer et al., 1999). The vertical flux formulation results from letting the sedimentation and the advection term go to zero in the governing transport equation and assuming the remaining mechanism is vertical diffusion or flux of dust. The vertical flux of dust F_a is then,

$$F_a = -\kappa u_* z \frac{\partial c}{\partial z}, \tag{1}$$

where c is the concentration of dust, κ is the von Karman constant, u_* is the friction velocity, and z is the height from the surface. A negative concentration gradient results in a flux of dust away from the surface. This simplification for the flux is only valid over idealized flat terrain where the turbulence in the boundary layer is adequately described by u_*. The vertical flux equation can be written discretely to evaluate individual measurement from a meteorological tower as follows:

$$F_a = -k u_* z_2 \frac{C_a(z_2 + \Delta z; x) - C_a(z_2 - \Delta z; x)}{2\Delta z}, \tag{2}$$

where z_2 represents a vertical reference point from which concentrations C_a are measured at equally spaced vertical distances Δz apart. With this method only two vertical measurement locations are needed in the field to make an estimation of the vertical flux. This formulation, however, is highly dependent on vertical gradients of concentration. Large emissions local to the monitoring tower suggest a large source of potential emissions; however, emissions upwind of these measurements could also influence the result. Gillette and Goodwin (1974) note a case where a negative aerosol flux was observed using this methodology, possibly, due to a "higher rate of

erosion upwind of the sampling tower than near the tower''. Thus, in this case, the ineffectiveness of the formulation results from a failure of the experiments to satisfy the assumption that advection is negligible.

The vertical flux approach to emissions is ubiquitous in the current literature, both in field, modeling, and wind-tunnel studies (Chepil, 1945; Cowherd and Ono, 1990; Stetler and Saxton, 1996; Borrmann and Jaenicke, 1987; Fairchild and Tillery, 1982). In several of these studies, the horizontal sand saltation flux has been measured as well as a means to quantify the effect of saltation on the vertical flux of dust. In this paper we will use the vertical flux of dust to provide a comparison between our data and existing field data.

2. Experimental methods

2.1. Soil collection rationale and preparation

The details of soil collection rationale at Owens (dry) Lake and soil preparation are given in Roney and White (2004). In brief, Owens (dry) Lake areas previously shown to be sources of high emission were chosen for wind-tunnel soils testing. An effort to collect loose elastic soils of the same soil texture and similar size distributions at each site was made by collecting only those soils that were loose, sands or those under the thin crusts on the playa. The GPS coordinates, map locations, and descriptions of the soils are given in Roney and White (2004). For identification in the laboratory, the four soils were given names related to the location of collection as shown in Table 1. Nearly 5 t of soil from these locations was transported back to the University of California at Davis for the laboratory wind tunnel testing. Once at the University of California at Davis, they were prepared in a manner to represent the most emissive conditions; they were air dried, and if present, major aggregate clumping was eliminated with a coarse sieve. Random samples from each of the soil types were tested for chemical nature and texture as well as size distributions. The size distributions were consistent for each soil type and an average size distribution for each soil is shown in Roney and White (2004).

2.2. Wind tunnel

All measurements were made in the saltation wind tunnel (SWT), an environmental boundary layer wind tunnel at the University of California at Davis (Kim et al., 2000). This open-circuit wind tunnel is designed to simulate particle flows or saltation movement, and thus, is ideal for simulating the emission of dust from crustal surfaces such as Owens (dry) lake. The inlet of the wind tunnel has an array of flow straightening tubes to eliminate any large-scale turbulence resulting from objects in the surrounding room allowing the flow to develop naturally in the wind tunnel. Following the inlet, the tunnel has a 5 m section to develop a turbulent boundary layers characteristic of the flow near the surfaces of desert playas. In this section, pebbles attached to the bottom surface were evenly spaced but randomly oriented such that a well-developed two-dimensional turbulent boundary layer formed prior to impinging on the 5 m long soil bed. Within the sections containing the soil of interest, the boundary layers were closely matched due to similar roughness characteristics. To maintain an even depth of soil of approximately 30 mm, a trough running down the centerline of the wind-tunnel with dimensions $0.025\,\mathrm{m} \times 0.30\,\mathrm{m}$ was used. The side surfaces were covered with sand paper to match the roughness of the soils (Fig. 1). This depth of soil allowed for about 5 to 10 min of testing at lower speeds before appreciable amounts of soils were lost. Because of the soil loss, the maximum velocity tested in the wind tunnel could not exceed values of $14.0\,\mathrm{m\,s^{-1}}$. Lastly, the diffuser section opened to the outside atmosphere expelling any suspended dust or sand.

Table 1
Global positioning system (GPS) locations for the four soils collected at Owens (dry) Lake

Desig.	Description	Suspected type	GPS lat.	GPS long.
Soil #1	Old Pipe Line, Loamy Sand	Emissive soil	36°28.808 N	117°54.649 W
Soil #2	North Sand, Sand	"Sand"	36°29.194 N	117°54.655 W
Soil #3	Dirty Socks Dune, Sand	"Sand"	36°20.391 N	117°57.681 W
Soil #4	UCD Fence, Sandy Loam	Emissive soil	36°21.411 N	117°57.467 W

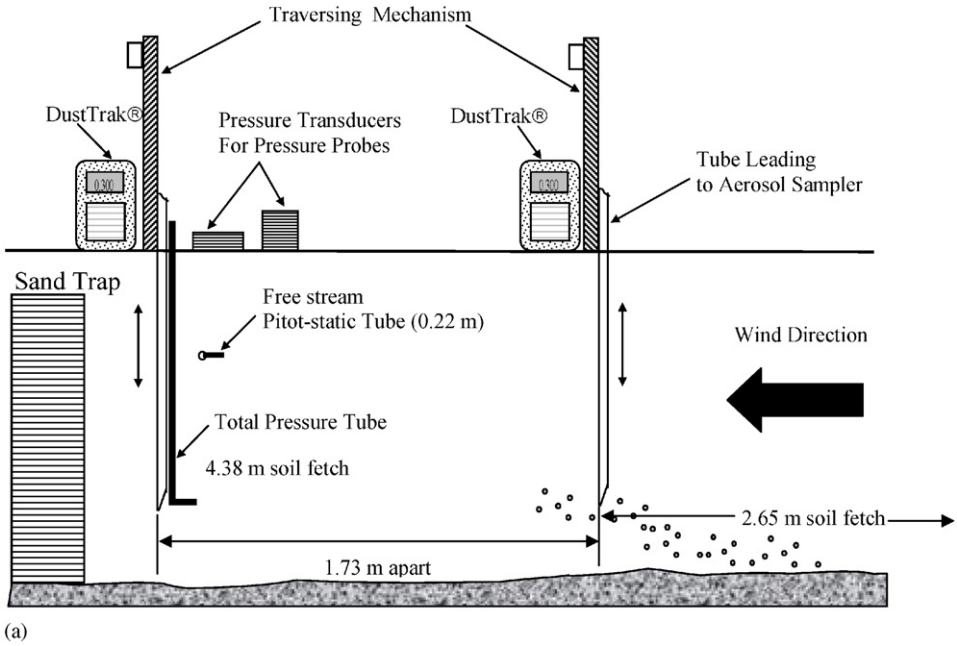

Fig. 1. Measurement set-up for testing emissions of loose soils: (a) a schematic; and (b) a photograph showing the soil bed which the emissions were measured over.

The wind-tunnel measurement instrumentation consisted of two TSI DustTraks® to measure PM_{10} aerosol concentrations (“fugitive dust”), a traversing total pressure probe to measure the vertical velocity, a Pitot-static probe to measure the mean free-stream velocity U_{ref} (located at 0.22 m above the surface), and stackable isokinetic sand traps (White, 1982) to measure the horizontal sand saltation flux. At this point it is important to state the TSI DustTrak® is not a federal reference method (FRM) or equivalent method for PM_{10}; however, for this study, the Great Basin Unified Air Pollution Control District (GBUAPCD) compared their DustTrak® to the tapered element oscillating microbalance (TEOM) samplers (an equivalent method) at three sites at Owens Lake, and consistently, the DustTrak® read approximately 50% of the TEOM value. In Ono et al. (2000), a comparison was performed between the TEOM and FRM samplers at Owens (dry) Lake. The FRM sampler values ranged from 60% to 106% of the TEOM values, so the factory calibration of the DustTrak® with Arizona Test Dust seems to be a reasonable approximation for dust-types at Owens (dry) Lake.

2.3. Loose soil emission measurements

Once the boundary layer flows were sufficiently established in the wind tunnel, the loose soil emission rates were measured for values above the threshold friction velocity u_{*t}. With the soil in place, emission rates were obtained experimentally by instantaneously measuring velocity and concentrations by simultaneously vertically traversing two DustTraks® and a total pressure probe at 2.65 and 4.38 m from the leading edge of the soil bed for a set of the same 10 heights (Fig. 1). The DustTraks® recorded concentration at each location in $\mathrm{mg\,m^{-3}}$ with the data acquired by an A/D board attached to a PC at a sampling rate of 1 Hz. At each traversing height measurements were taken for 10 s; these sampling times were used to give a sufficient number of measurements while allowing the test to be completed in less than five minutes maintaining a "steady" process. To obtain an emission rate, a control volume analysis was used between the various inlet and outlet measurements (Fig. 2). The emission rate was defined as the mass emitted in a unit area per unit time, $[\mathrm{M\,L^{-2}\,T^{-1}}]$ or $[\mathrm{mg\,m^{-2}\,s^{-1}}]$. The control volume was defined as $W_b \times L_b \times H_t$ where W_b is the width of the soil bed, L_b is the length of the soil bed or length between probes, and H_t is the height of the tunnel. The mass flux out of the control volume was defined as $\dot{m}_{out}$ and the mass flux in as $\dot{m}_{in}$, where "in" and "out" are relative to the control volume. The emission rate $\dot{E}$ for the control area, $A_b = W_b \times L_b$, was found by applying a mass balance on the control volume:

$$\dot{E} = \frac{1}{A_b}(\dot{m}_{out} - \dot{m}_{in}). \tag{3}$$

Since the aerosol sampler measures concentrations, the mass flux rates were described as a function of concentration:

$$\dot{m}_{out} = \int_0^{H_t} c_{out} u_{out} W_b \, dz, \tag{4}$$

$$\dot{m}_{in} = \int_0^{H_t} c_{in} u_{in} W_b \, dz, \tag{5}$$

where u and c represent the velocity and concentration 10-s averages. The c-subscripts represent entrance ("in") and exit ("out") locations. z is the direction away from the surface. The revised emission rate equation is

$$\dot{E} = \frac{1}{L_b}\int_0^{H_t} (c_{out} u_{out} - c_{in} u_{in}) \, dz. \tag{6}$$

For a simplified analysis, emissions upwind of the soil bed were assumed to be zero. This assumption is based on measurements of dust concentrations in the inlet of the wind tunnel that showed that the incoming air had negligible amounts of dust relative to the measurements above the soil bed. Likewise, the velocity profiles are assumed equivalent at the entrance and exit of the control volume. Testing showed that velocity profiles measured simultaneously at 2.65 and 4.38 m were similar. Once the velocity and concentration profiles were obtained, emission rates were calculated from Eq. (6). Regression curves were fit to each PM_{10} concentration profile and velocity curve. The product of the two was integrated numerically to obtain an emission rate per unit area $\dot{E}$. This procedure was repeated for numerous free-stream wind-tunnel velocities ranging from 8.5 to $14.0\,\mathrm{m\,s^{-1}}$ and corresponding to different u_* friction velocity values ranging from 0.35 to $1.1\,\mathrm{m\,s^{-1}}$ for each soil. Typical turbulent boundary layer heights δ at the measurement locations ranged from 22 to 25 cm. The emission rate measurements were replicated for

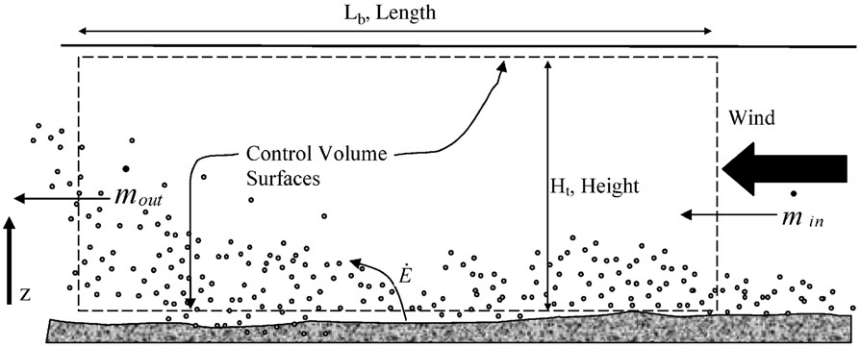

Fig. 2. Schematic representing the method of determining loose soil emission rates with a control volume.

ranges of u_* for each soil; the number of replications varied from one to four. However, data-acquired measurements were made during each test giving multiple measurements of individual quantities during the test as well. Determination of the roughness height z_0, the friction velocity u_*, and the Coefficient of Drag C_d of each surface is discussed in Roney and White (2004) in detail. Both z_0 and u_* are determined by using mixing length theory for turbulent boundary layers that have roughness in combination with experimental results; z_0 is determined from velocity profiles prior to threshold, and u_* is related to the slope of the profiles. The C_d of the surface is calculated from the "prethreshold" linear relationship of u_* versus the reference free-stream velocity U_{ref}. The concentration profile results also contain information on the vertical flux of dust F_a which was evaluated as previously shown in Gillette and Walker (1977), and Borrmann and Jaenicke (1987). F_a is compared to the emissions data in other published studies.

The sand flux was obtained simultaneously for several of the experiments by using 15–21 sand traps stacked on top of each other. Each of these traps was 2.0 cm high by 1.0 cm wide and had a frontal sampling area of 0.0003 m^2. The traps were placed at the exit of the test section near the diffuser with the frontal area perpendicular to the wind velocity. The horizontally moving mass greater than 40 μm aerodynamic diameter was collected in the traps. The traps are approximately isokinetic samplers as the air moves freely through the sampler at approximately the same rate as the wind velocity (White, 1982). The time t_s of collection was recorded, and the mass in each trap was weighed. A sand flux was obtained in the following way at each height:

$$q_i = \frac{m_i}{t_s A_i}, \tag{7}$$

where m_i is the mass collected in each sand trap at each location, A_i is the frontal area of the trap, and t_s is the time of collection. Once the sand flux had been obtained, a total flux was obtained with the following equation:

$$Q = \sum_{i=1}^{21} q_i h_i, \tag{8}$$

where h_i is the height of the trap. This sand flux was an indication of the saltation rate for various wind velocities for each soil.

In addition, the ratio of horizontal PM_{10} flux to total horizontal mass flux was obtained from the emission rates and sand flux rates. Gillette et al. (1997a) use the ratio of the vertical flux of dust F_a to the total horizontal mass flux to describe field measured emissions at Owens (dry) Lake. A comparison between the wind-tunnel measured vertical flux of dust F_a to the total horizontal mass flux ratio was also compared with this field study.

3. Results

3.1. PM_{10} loose soil emission rates

Velocity profiles were obtained for each saltation case during emissions testing. Above threshold conditions, there is no longer a focus of profiles to z_0, since movement of the soil causes an increased effective roughness due to saltating particles and ripples. For each increase in free-stream velocity, there is a different z-intercept which is denoted z_0'. However, there is a new focus of the velocity profiles denoted as z' with a corresponding off-set velocity U_z'. Bagnold (1941) found a similar result for his velocity profiles in his experiments on sand movement. A sample velocity profile plot for one of the four soils is shown in Fig. 3.

Simultaneously, PM_{10} concentration profiles were obtained for several cases at 2.65 and 4.38 m from the beginning of the soil bed. Typical data for one experimental test are shown in Fig. 4. The data were curve-fit to expedite the integration, with the typical curve-fit for the concentration profiles having a power-law form $C = az^{-b}$ where C is the concentration and "a" and "b" are fitting coefficients (an occasional fit was of the form $C = d_0 e^{-d_1 z}$ where d_0 and d_1 are fitting coefficients). Likewise, the velocity profiles were fit with "law-of-wall" type fits typical of turbulent boundary layer profiles. These fits are shown in Fig. 5. The integration as specified in Eq. (6) was done with a discrete numerical technique (trapezoidal rule) and the limits of integration taken between 0.01 and 0.5 m with $\Delta z = 0.01$ m. For the concentration profiles, extending the curve-fit beyond the region of the data near the surface posed the possibility of introducing erroneous mass, since the true tendency very near the surface (less than 0.01 m) is typically for the profile to saturate and not follow the power-law fit. Using these results and Eqs. (3)–(6) emissions rates and horizontal PM_{10} fluxes were calculated.

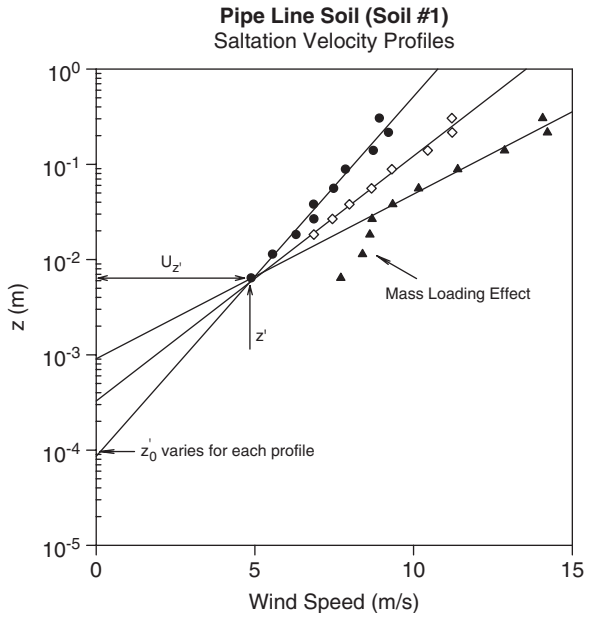

Fig. 3. Sample velocity profiles for the cases when the soil is being blown and transported. For each increase in free-stream velocity, there is a different z-intercept which is denoted z_0', and there is a new focus of the velocity profiles denoted as z' with a corresponding off-set velocity $U_{z'}$.

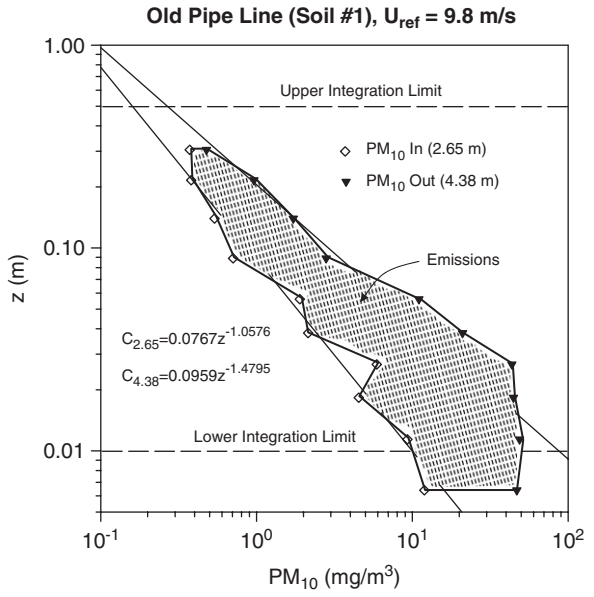

Fig. 4. The simultaneous PM_{10} concentration profiles for Soil #1 at $U_{ref} = 9.8\,m\,s^{-1}$ for both the 2.65 m fetch and the 4.38 m fetch distance. There is a significant gain in the concentration levels between the two probes.

For these cases, PM_{10} horizontal flux values at $x = 2.65$ m could be compared to values at $x = 4.38$ m in effect looking at the fetch effect on emissions. Two

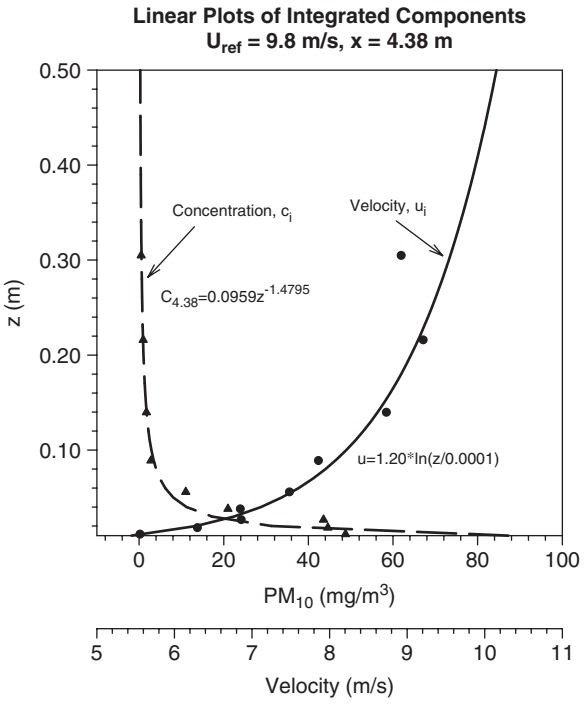

Fig. 5. Simultaneous velocity and concentration profiles obtained at $x = 4.38$ m in the wind tunnel. These profiles are then used to obtain an emission rate for the wind-tunnel measurements.

different types of results occur in this comparison; first, those where there is distinctly increasing amounts of PM_{10} along the length of the soil test bed between 2.65 and 4.38 m (Fig. 4), and second, those where the PM_{10} levels remain about the same or even decrease slightly. For the majority of the test cases at the highest velocities, the difference in horizontal mass between 2.65 and 4.38 m locations is small (Fig. 6). Thus, if we take the control volume between 2.65 and 4.38 m there is no emission rate or a negative emission rate. At first, this posed a perplexing question as previous studies (Gillette et al., 1996) suggests that due to the Owen effect the mass should increase substantially along the fetch.

An initial conceptual model based on these observations was developed indicating how these situations may arise (Fig. 7): at lower velocities the horizontal mass gain is approximately linear with increasing fetch; however, at higher velocities the wind tunnel height and near-surface mass saturation becomes a limitation on how much additional mass can become entrained. The saturation effect is a result of high mass concentrations of fine particles in the wind-tunnel air at the measurement location both at the surface and in the

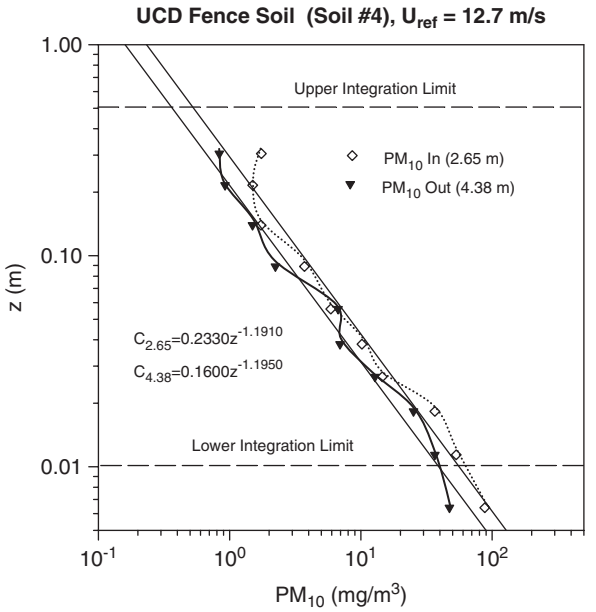

Fig. 6. The simultaneous PM_{10} concentration profiles for Soil #4 at $U_{ref} = 12.7\,m\,s^{-1}$ for both the 2.65 m fetch and the 4.38 m fetch distance. In this case, the concentration levels between the two probes remain about the same. The lines are the curve fits to the concentration profiles.

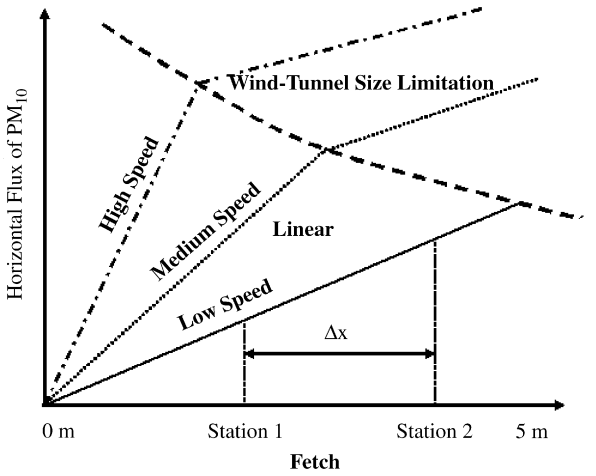

Fig. 7. A conceptual model for determining the emission rates in the wind tunnel is presented. The wind-tunnel size (the height) is considered a limitation on the naturally evolving emission for the highest speeds. The emissions rates should thus if possible be calculated in regions were there is nearly linear gain in emissions.

free-stream air. The air may be saturated in the wind-tunnel compared to natural conditions for a particular location, because we are confining the emission mechanism between the wind-tunnel walls during strong emissive conditions. In "nature" we would see continued upward diffusion. With near-surface saturation, the turbulent diffusion mechanism near the surface decreases due to increase mass loading near the surface; this may occur in "nature" as well. Also, with deposition the concentrations may drop. No significant deposition was observed on the wind-tunnel walls as strong advection transported the particles downstream; however, decreases in the near surface entrainment mechanism may have allowed deposition on the surface. So, saturation may occur for two reasons: (1) significant mass at the surface affecting the diffusion mechanism and/or (2) the wind-tunnel height limits the amount of upward mixing during strong turbulent diffusion. Experimental results verifying this conceptual model are shown in Fig. 8. Based on this conceptual model, the emission rates were calculated in the linear region or between the beginning of soil bed and the position of the last profile.

For all the loose soil emission measurements, the control volume was taken as the beginning of the bed $x = 0$–4.38 m; $L_b = 4.38$ m in Eq. (6) where $\dot{m}_{out}$ can be calculated and $\dot{m}_{in} = 0$ at the beginning of the bed ($x = 0$). This method of calculation provides an average emission rate over the entire soil bed as given in Tables 2–5. Likewise, a similar calculation was performed for cases where concentration profiles were measured at $x = 2.65$ m such that the

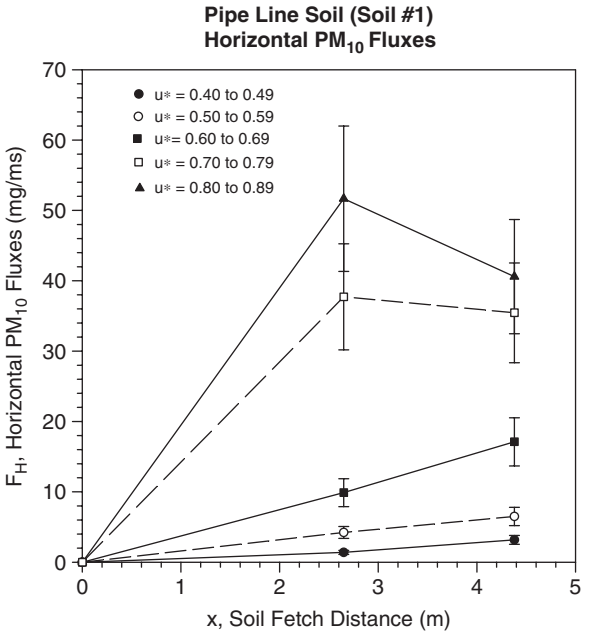

Fig. 8. A sample experimental study of the horizontal flux shows that the emissions follow very closely to the conceptual model. Plots of the horizontal flux for the other three soils show a comparable result.

exit mass is calculated at $x = 2.65$ m and $\dot{m}_{in} = 0$. The results for these cases are given in Tables 6–9.

The values shown in the tables are average estimates for all the studies conducted with a loose "dry" soil. The highest emission rates measured were 20 000–25 000 $\mu g\,m^{-2}\,s^{-1}$ for the "emissive soils", Soil#1 and Soil#4. However, for the UCD Fence Soil (Soil #4) the 25 000 $\mu g\,m^{-2}\,s^{-1}$ seems to lie outside the realm of the rest of the data for that soil-type. However, homogeneity of soils within sample locations is assumed, and it possible that the soil used in this test differed slightly. Over all, the Pipe Line Soil (Soil #1) from the North appears to be the most "emissive" of the four soil types. A sample plot showing the estimated emission rates and trends for the North Soils is shown in Fig. 9. Calculations likes those presented in this plot are shown for the other soils in the tables.

The most surprising result is that Dirty Socks Dune Sand (Soil #3) contains a high amount of PM_{10} and is nearly as emissive as the "emissive" soils at the lower u_* values. At Owens (dry) Lake, this may result from the deposition of PM_{10} in the sand due to northerly wind storm events in which large amounts of PM_{10} from the UCD Fence Soil (Soil #4) fall-out over the sand and become integrated among the grains of sand. This result indicates that Soil #3 could potentially be a large source of emissions during storms on Owens (dry) Lake. At the higher u_* values the Dirty Socks Sand emissions levels off, possibly, due to sand ripples offering protection that limits increases in the dust emissions.

Table 2
Calculated "loose" soil emission rates and vertical fluxes for the Pipe Line Soil (North Soil) at $x = 4.38$ m from the wind-tunnel measurements

Desig.	u_* ($m\,s^{-1}$)	U_{ref} ($m\,s^{-1}$)	$u(10\,m)$ ($m\,s^{-1}$)	$\dot{E}$ (PM_{10}) ($\mu g\,m^{-2}\,s^{-1}$)	F_a (PM_{10}) ($\mu g\,m^{-2}\,s^{-1}$)
Soil #1	0.47	9.0	12.7	81.5	74.8
Soil #1	0.48	9.6	13.4	33.0	20.0
Soil #1	0.49	10.4	14.0	103.0	109.8
Soil #1	0.50	9.8	13.8	2600	5280
Soil #1	0.57	10.3	15.1	176.0[a]	281[a]
Soil #1	0.61	10.6	15.4	5920	9290
Soil #1	0.71	11.3	17.2	4580	8980
Soil #1	0.76	11.2	18.1	5040	10 130
Soil #1	0.78	11.3	18.1	15 200[a]	27 340[a]
Soil #1	0.80	11.32	18.5	7560	14 050
Soil #1	1.12	14.2	24.3	19 420	41 170

[a]Data points marked are unusually high or low, and thus, were not used in the plots.

Table 3
Calculated "loose" soil emission rates and vertical fluxes for the North Sand (North Soil) at $x = 4.38$ m from the wind-tunnel measurements

Desig.	u_* ($m\,s^{-1}$)	U_{ref} ($m\,s^{-1}$)	$u(10\,m)$ ($m\,s^{-1}$)	$\dot{E}$ (PM_{10}) ($\mu g\,m^{-2}\,s^{-1}$)	F_a (PM_{10}) ($\mu g\,m^{-2}\,s^{-1}$)
Soil #2	0.47	9.1	13.2	52.0	86.6
Soil #2	0.48	8.9	13.0	24.9	23.7
Soil #2	0.53	10.3	14.4	137	200
Soil #2	0.53	10.1	14.4	103	246
Soil #2	0.59	10.6	15.7	393	493
Soil #2	0.59	10.1	14.6	384	1090
Soil #2	0.65	11.3	16.7	449	514[a]
Soil #2	0.76	11.6	17.9	1200	3330
Soil #2	0.85	12.9	19.9	1180	3020
Soil #2	0.98	13.0	21.5	1280[a]	3810
Soil #2	1.00	13.0	21.6	3388	7020

[a]Data points marked are unusually high or low, and thus, were not used in the plots.

Table 4
Calculated "loose" soil emission rates and vertical fluxes for the Dirty Socks Sand (South Soil) $x = 4.38$ m from the wind-tunnel measurements

Desig.	$u*$ (m s^{-1})	U_{ref} (m s^{-1})	u(10 m) (m s^{-1})	$\dot{E}$ (PM_{10}) (μg m^{-2} s^{-1})	F_a (PM_{10}) (μg m^{-2} s^{-1})
Soil #3	0.56	9.9	14.3	25.2	34.6
Soil #3	0.58	9.0	14.3	48.5	8.9
Soil #3	0.61	9.9	15.2	1120	2370
Soil #3	0.67	11.2	16.7	1620	2010
Soil #3	0.68	11.5	17.5	1920	2890
Soil #3	0.75	11.4	18.1	783[a]	862[a]
Soil #3	0.79	12.9	19.4	2660	3190
Soil #3	0.84	12.6	19.1	2580	3890
Soil #3	1.01	12.5	21.6	3640	7090
Soil #3	1.02	13.0	22.1	3015	5290
Soil #3	1.09	13.6	23.4	3731	6920

[a]Data points marked are unusually high or low, and thus, were not used in the plots.

Table 5
Calculated "loose" soil emission rates and vertical fluxes for the UCD Fence Soil (South Soil) at $x = 4.38$ m from the wind-tunnel measurements

Desig.	$u*$ (m s^{-1})	U_{ref} (m s^{-1})	u(10 m) (m s^{-1})	$\dot{E}$ (PM_{10}) (μg m^{-2} s^{-1})	F_a (PM_{10}) (μg m^{-2} s^{-1})
Soil #4	0.35	8.5	11.1	35.4	5.5
Soil #4	0.42	9.9	13.2	223	138
Soil #4	0.49	10.5	14.3	2230	1440
Soil #4	0.51	8.9	13.2	20.0[a]	22.3[a]
Soil #4	0.56	11.6	16.3	1871	2400
Soil #4	0.63	13.1	18.7	1342	1890
Soil #4	0.67	11.7	17.0	497[a]	1,280
Soil #4	0.69	11.6	17.6	3637	8490
Soil #4	0.69	13.0	19.0	2434	3770
Soil #4	0.70	13.7	20.0	3055	2270
Soil #4	0.71	12.7	19.0	2550	4140
Soil #4	0.75	12.7	19.1	9480[a]	21 460[a]
Soil #4	0.86	13.9	21.7	13 740[a]	21 990[a]
Soil #4	0.90	13.8	22.0	9850	21 950[a]

[a]Data points marked are unusually high or low, and thus, were not used in the plots.

Table 6
Calculated "loose" soil emission rates and vertical fluxes for the Pipe Line Soil (North Soil) at $x = 2.65$ m from the wind-tunnel measurements

Desig.	$u*$ (m s^{-1})	U_{ref} (m s^{-1})	u(10 m) (m s^{-1})	$\dot{E}$ (PM_{10}) (μg m^{-2} s^{-1})	F_a (PM_{10}) (μg m^{-2} s^{-1})
Soil #1	0.47	9.0	12.7	22.3	—
Soil #1	0.50	9.8	13.8	1030	498
Soil #1	0.61	10.6	15.4	3730	2890
Soil #1	0.78	11.3	18.1	24 800[a]	35 670[a]
Soil #1	0.80	11.32	18.5	14 200	16 600

[a]Data points marked are unusually high or low, and thus, were not used in the plots.

Unusually low or high points were systematically eliminated to form clearer plots and are marked by an asterisk in Tables 2–9. These data points are left in the tables for completeness as they may be suggestive of the variability within some of the soil types. In addition, all the Tables include an

Table 7
Calculated "loose" soil emission rates and vertical fluxes for the North Sand (North Soil) at $x = 2.65$ m from the wind-tunnel measurements

Desig.	u_* (m s^{-1})	U_{ref} (m s^{-1})	u(10 m) (m s^{-1})	$\dot{E}$ (PM_{10}) (μg m^{-2} s^{-1})	F_a (PM_{10}) (μg m^{-2} s^{-1})
Soil #2	0.44	9.2	12.2	95.6	34.0
Soil #2	0.48	8.9	13.0	38.3	11.0
Soil #2	0.53	10.0	14.2	370	273
Soil #2	0.59	10.1	14.6	400	732
Soil #2	0.69	11.8	17.2	960	837
Soil #2	0.76	11.6	17.9	1680	3780[a]
Soil #2	0.85	12.9	19.9	1230	1690
Soil #2	0.90	12.8	20.6	1250	1740
Soil #2	0.98	13.0	21.5	1660	3360

[a]Data points marked are unusually high or low, and thus, were not used in the plots.

Table 8
Calculated "loose" soil emission rates and vertical fluxes for the Dirty Socks Sand (South Soil) at $x = 2.65$ m from the wind-tunnel measurements

Desig.	u_* (m s^{-1})	U_{ref} (m s^{-1})	u(10 m) (m s^{-1})	$\dot{E}$ (PM_{10}) (μg m^{-2} s^{-1})	F_a (PM_{10}) (μg m^{2} s^{-1})
Soil #3	0.32	8.4	10.4	9.2	0.5
Soil #3	0.40	9.3	11.9	22.7	28.3
Soil #3	0.58	9.0	14.3	89.2	19.1
Soil #3	0.61	9.9	15.2	670	975
Soil #3	0.61	11.1	16.3	790	603
Soil #3	0.68	11.5	17.5	3200	4390
Soil #3	0.71	12.8	18.9	3770	5000
Soil #3	0.75	12.9	19.4	4330	6310
Soil #3	0.79	12.9	19.4	5190	6260
Soil #3	0.84	12.6	19.1	4460	6160

Table 9
Calculated "loose" soil emission rates and vertical fluxes for the UCD Fence Soil (South Soil) at $x = 2.65$ m from the wind-tunnel measurements

Desig.	u_* (m s^{-1})	U_{ref} (m s^{-1})	u(10 m) (m s^{-1})	$\dot{E}$ (PM_{10}) (μg m^{-2} s^{-1})	F_a (PM_{10}) (μg m^{-2} s^{-1})
Soil #4	0.35	8.5	11.1	14.7	3.0
Soil #4	0.39	9.4	11.9	174	6.2
Soil #4	0.42	9.9	13.2	240	8.7
Soil #4	0.48	9.9	13.6	379	216
Soil #4	0.49	10.5	14.3	1720	384
Soil #4	0.52	11.0	14.7	1120	440
Soil #4	0.56	11.6	16.3	2980	2926
Soil #4	0.63	13.1	18.7	2060	1860
Soil #4	0.66	12.2	17.0	2350	3190
Soil #4	0.69	13.0	19.0	2660	2500
Soil #4	0.70	13.7	20.0	3670	3340
Soil #4	0.71	12.7	19.0	6070	5930
Soil #4	0.76	12.9	19.2	4240	7110
Soil #4	0.78	13.1	19.5	4140	5630

equivalent wind value for 10 m heights. This velocity is calculated by an extension of the law-of-the-wall boundary layer profiles.

All of the soils at the highest wind-tunnel speeds rapidly formed ripple beds. The wind forms ridges of sorted particles that are well established very

quickly in the tunnel. Since these beds are formed so rapidly, there is no need to consider their time dependence and their effect on the flow after the initial sorting. The time constant for the initial sorting was estimated at 100 s from start-up of the wind tunnel to formation of "steady" ripples. Analysis shows that some of the initial points in the profiles were taken before this time constant was exceeded. However, these points usually appeared erroneous or saturated in the profiles and the fits did not include these data points; therefore, the profiles seem to be an accurate representation of the "steady-state" emission process with well-formed ripples. A caution then is that the profiles presented in this paper may not capture an initial "blow-off" of dust which is highly time dependent, and could possibly be another source of high, however, non-sustained emissions.

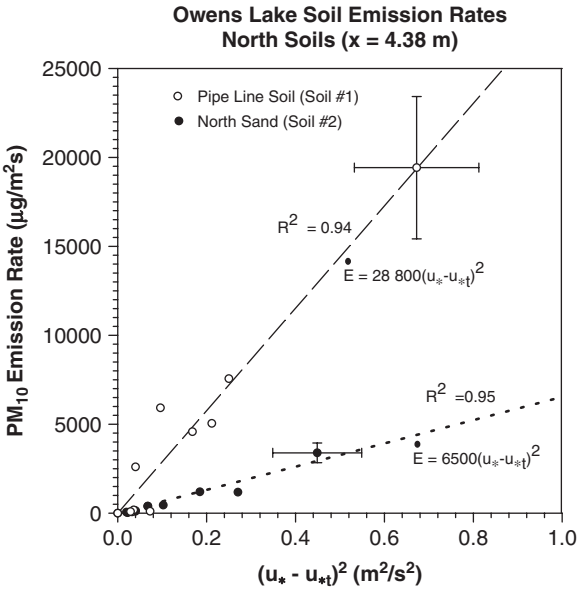

Fig. 9. A plot for the north soil emission rates showing the rates are related to the friction velocity squared (or the shear velocity). Comparable plots were made for the other soil cases as well. The error bars represent the uncertainty associated with the measurement and the calculation.

3.2. PM_{10} emissions with upwind saltation

The analysis of the last section was reproduced with Eqs. (3)–(6) for cases with "naturally" occurring upwind saltation: the first bed of "emissive soil" in the wind tunnel was replaced with a bed of natural sand particles from Owens (dry) Lake, either with the north sands or south sands closest to the emissive soil location. For the south sand blowing over the "UCD Fence Soil", the simulation was termed "South Sheet", and for the north sand blowing over the "Pipeline Soil", the simulation was termed "North Sheet". For these cases, the control volume was taken as the volume between the 2.65 m probe and the 4.38 m probe. The integrated profiles at each location were subtracted from each other and divided by $L_b = 1.73$ m, in effect capturing those emissions that were due to the soil bombardment by sand particles and not those pertaining to the sand movement before the emissive bed. In this way, the advected upwind dust concentrations from the sand were eliminated in the calculation. The results are shown in Tables 10 and 11. Table 11 shows the emissions at $x = 2.65$ m from the upwind sands.

Saltation has marked effect on the emission rate as exemplified in the North Sheet simulation shown in Figs. 10 and 11 where there is an abrupt transition from sand emissions to soil emissions. This enhancement is likely due to sand particles

Table 10
Calculated emission rates and vertical fluxes for enhanced saltation for the north and south soils at $x = 4.38$ m from the wind-tunnel measurements

Desig.	Descrip.	u_* (m s^{-1})	U_{ref} (m s^{-1})	u(10 m) (m s^{-1})	$\dot{E}$ (PM_{10}) (μg m^{-2} s^{-1})	F_a (PM_{10}) (μg m^{-2} s^{-1})
Soil #2 over Soil #1	North Sheet	0.44	9.2	12.2	239	231
Soil #2 over Soil #1	North Sheet	0.53	10.0	14.2	1975	2654
Soil #2 over Soil #1	North Sheet	0.69	11.8	17.2	11 600	11 900
Soil #2 over Soil #1	North Sheet	0.90	12.8	20.6	27 600	30 520
Soil #3 over Soil # 4	South Sheet	0.32	8.4	10.4	3.58	1.5
Soil #3 over Soil # 4	South Sheet	0.40	9.3	11.9	23.2	126
Soil #3 over Soil # 4	South Sheet	0.61	11.1	16.3	2920	2286
Soil #3 over Soil # 4	South Sheet	0.71	12.8	18.9	5640	7297
Soil #3 over Soil # 4	South Sheet	0.75	12.9	19.4	4620	8313

Table 11
Calculated emission rates for enhanced saltation for the north and south soils at $x = 2.65$ m from the wind-tunnel measurements

Desig.	Descrip.	u_*(m s^{-1})	U_{ref}(m s^{-1})	u(10 m) (m s^{-1})	$\dot{E}$(PM$_{10}$)(μg m^{-2}s^{-1})
Soil #2 over Soil #1	North Sand	0.44	9.2	12.2	95.6
Soil #2 over Soil #1	North Sand	0.53	10.0	14.2	370
Soil #2 over Soil #1	North Sand	0.69	11.8	17.2	960
Soil #2 over Soil #1	North Sand	0.90	12.8	20.6	1250
Soil #3 over Soil # 4	Dirty Socks Sand	0.32	8.4	10.4	9.2
Soil #3 over Soil # 4	Dirty Socks Sand	0.40	9.3	11.9	22.7
Soil #3 over Soil # 4	Dirty Socks Sand	0.61	11.1	16.3	790
Soil #3 over Soil # 4	Dirty Socks Sand	0.71	12.8	18.9	3770
Soil #3 over Soil # 4	Dirty Socks Sand	0.75	12.9	19.4	4330

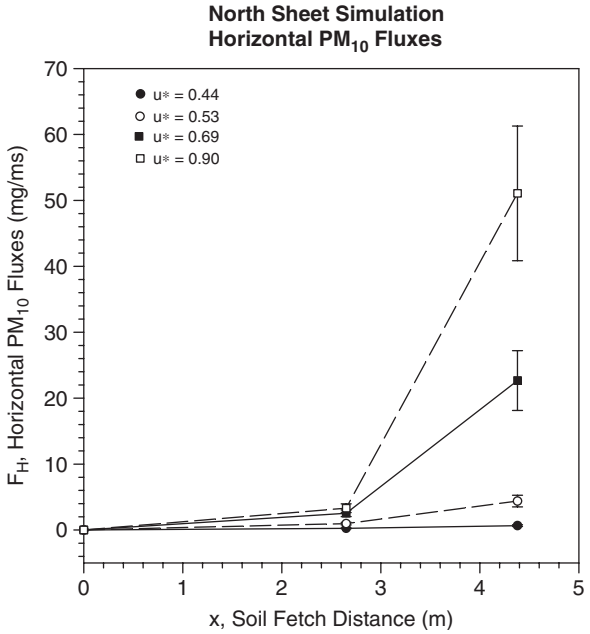

Fig. 10. A sample experimental study of the horizontal flux for the enhanced saltation studies of the north soils. A sharp delineation between the upstream sand and the pipe line soil emissions can be seen in this plot. In addition, the emissions become enhanced due to sand particles impacting the pipe line soil.

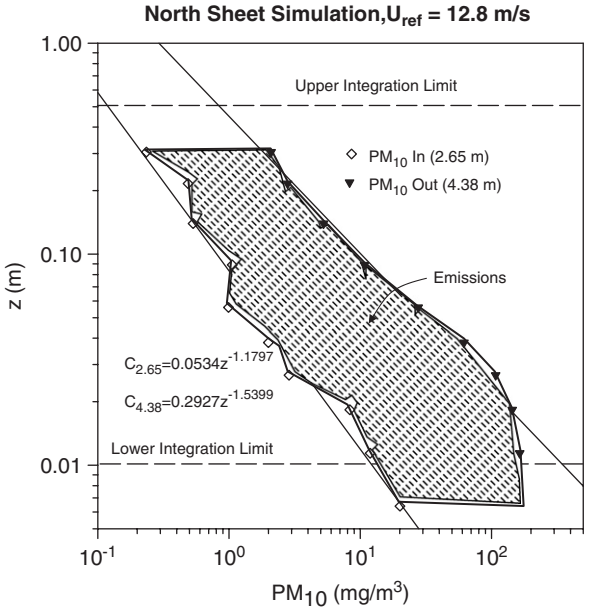

Fig. 11. The simultaneous PM_{10} concentration profiles for north sand saltating over pipe line soil at $U_{ref} = 9.8$ m s^{-1} for both the 2.65 m fetch and the 4.38 m fetch distance. There is a significant gain in the concentration levels between the two probes as shown corresponding to significant emissions.

impacting the soil with ballistic trajectories. These impacts eject PM_{10} into the air allowing it to more easily be entrained into the turbulent flow and be transported upward. In addition, agglomerations in the soil are likely abraded into smaller more emissive particles by the coarser saltating sand. In Fig. 12, the emission rates are plotted as before. In the plot, the sustained dust threshold friction velocity u_{*t} as calculated and presented in Roney and White (2004) are subtracted from the friction velocity u_*. The combined term is then squared such that the emissions begin approximately at zero. The enhancement in emission rates by introducing saltating sand upstream of the emissive soils is indicated by the trend lines in Fig. 12. The two sets of soils are presented with regards to their soil texture as well, and the soil texture appears to be a strong indicator of emissions as well.

3.3. Vertical dust fluxes

Eq. (2) was used to estimate a vertical flux of dust F_a from two points in each profile at both the $x = 2.65$ and 4.38 m fetch locations. A summary of

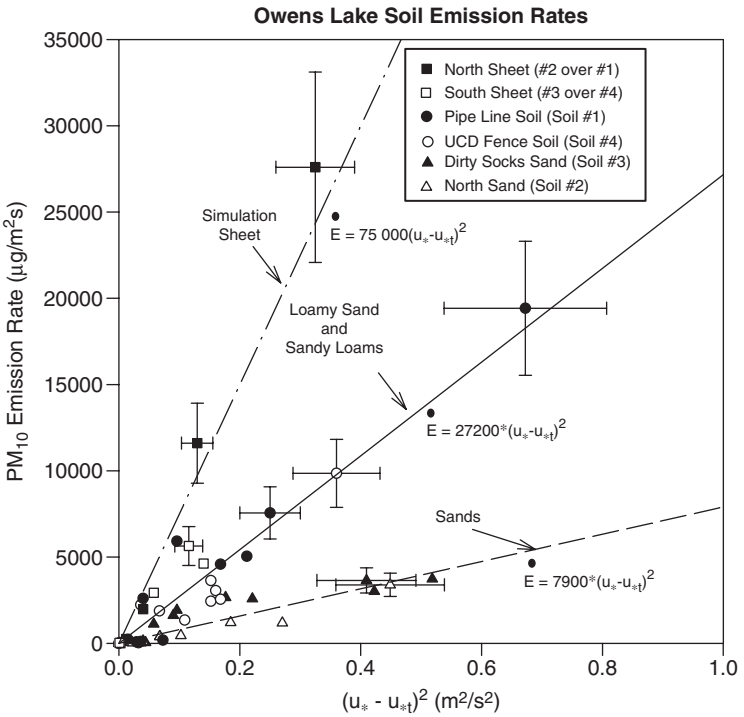

Fig. 12. The PM_{10} emission rates as a function of effective wind shear velocity squared for all the soils is shown above. The data is sorted by soil-type showing differences between the sands and "loamy" soils. Furthermore, the enhanced saltation (the sheet simulations) produces even more emissions. The error bars represent the uncertainty associated with the measurement and the calculation.

the values is given in Tables 2–9. Trends for the vertical fluxes are similar to those shown in Fig. 9 for the emission rate estimates. The similarity in trends indicates the vertical flux of dust is directly related to the horizontal flux of dust measured in the wind tunnel.

3.4. Sand fluxes

Total sand fluxes Q at approximately $x = 4.38$ m for selected cases were calculated from the mass collected using the sand traps. Profiles of the sand flux q at each height were obtained for each case as described in Eq. (7). The total sand fluxes calculated from these curves with Eq. (8) are given in Tables 12–17. The measurements indicate that all four soils had substantial amounts of saltating particles. Q for both cases of enhanced upwind saltation decreased slightly in comparison to this value for the saltating sand alone. The "loamy" soils had the lowest Q, but only slightly lower than the sands. Q are nearly equivalent for all cases, and increase with u_*. The slightly differing sand flux rates between soils at a given u_* can be directly attributed to the dust content again. A likely mechanism for this result is that "sand on sand" impacts are more elastic and movement is facilitated, while "sand on soil" collisions are more plastic and impede the momentum of the particles that are moving through the soil. Shao et al. (1993) note that "the sand particles are coated by dust and the cohesive forces between grains are greatly enhanced and the coefficient of restitution (crudely, the elasticity) of the bed is greatly reduced".

Finally, a ratio of horizontal PM_{10} flux F_H to the total soil flux q_{tot} (sand and dust) was calculated as shown in Fig. 13. Horizontal PM_{10} flux becomes a larger ratio of the total mass suspended as the friction velocity increases. High energy impacts of saltating particles are likely to play the role of abrading and breaking agglomerates. There is also significant difference between sand and the emissive soils as represented by the two trend lines. This ratio is very similar to the vertical flux to horizontal mass ratio.

3.5. Vertical flux to horizontal mass flux ratio

The vertical dust fluxes F_a estimated from the wind-tunnel concentration profiles along with q_{tot}

Table 12
Calculated total sand flux Q, horizontal PM_{10} flux F_H, and ratio of F_H to the total mass flux q_{tot} for the Pipe Line Soil (North Soil) from the wind-tunnel measurements

Desig.	u_* ($m\,s^{-1}$)	U_{ref} ($m\,s^{-1}$)	F_H (PM_{10}) ($g\,m^{-1}\,s^{-1}$)	F_a (PM_{10}) ($g\,m^{-2}\,s^{-1}$)	Q ($g\,m^{-1}\,s^{-1}$)	F_H/q_{tot}	F_a/q_{tot} (m^{-1})
Soil #1	0.48	9.6	0.00015	0.00002	0.33	0.00044	0.00006
Soil #1	0.49	10.4	0.00045	0.00011	1.23	0.00037	0.00009
Soil #1	0.57	10.3	0.00077	0.00028	1.12	0.00069	0.00025
Soil #1	0.71	11.3	0.02002	0.00900	17.20	0.00120	0.00052
Soil #1	0.76	11.2	0.02210	0.01013	13.17	0.00170	0.00077
Soil #1	1.12	14.2	0.08590	0.04120	51.44	0.00170	0.00080

Table 13
Calculated total sand flux Q, horizontal PM_{10} flux F_H, and ratio of F_H to the total mass flux q_{tot} for the North Sand (North Soil) from the wind-tunnel measurements

Desig.	u_* ($m\,s^{-1}$)	U_{ref} ($m\,s^{-1}$)	F_H (PM_{10}) ($g\,m^{-1}\,s^{-1}$)	F_a (PM_{10}) ($g\,m^{-2}\,s^{-1}$)	Q ($g\,m^{-1}\,s^{-1}$)	F_H/q_{tot}	F_a/q_{tot} (m^{-1})
Soil #2	0.47	9.1	0.00023	0.00009	1.72	0.00013	0.00005
Soil #2	0.48	8.9	0.00011	0.00002	1.41	0.00008	0.00002
Soil #2	0.53	10.3	0.00060	0.00020	3.93	0.00015	0.00005
Soil #2	0.53	10.1	0.00045	0.00025	2.92	0.00015	0.00008
Soil #2	0.59	10.6	0.00168	0.00049	11.64	0.00014	0.00009
Soil #2	0.59	10.1	0.00238	0.00109	6.73	0.00035	0.00007
Soil #2	0.65	11.3	0.00196	0.00051	5.36	0.00037	0.00010
Soil #2	0.76	11.6	0.00526	0.0033	31.42	0.00017	0.00011
Soil #2	0.85	12.9	0.00517	0.00302	33.52	0.00015	0.00009
Soil #2	0.98	13.0	0.00560	0.00381	31.69	0.00018	0.00012
Soil #2	1.00	13.0	0.01480	0.00702	34.40	0.00043	0.00020

Table 14
Calculated total sand flux Q, horizontal PM_{10} flux F_H, and ratio of F_H to the total mass flux q_{tot} for the enhanced saltation of north soils from the wind-tunnel measurements

Desig.	u_* ($m\,s^{-1}$)	U_{ref} ($m\,s^{-1}$)	F_H (PM_{10}) ($g\,m^{-1}\,s^{-1}$)	F_a (PM_{10}) ($g\,m^{-2}\,s^{-1}$)	Q ($g\,m^{-1}\,s^{-1}$)	F_H/q_{tot}	F_a/q_{tot} (m^{-1})
Soil #2 over #1	0.44	9.2	0.00067	0.00023	1.76	0.00038	0.00013
Soil #2 over #1	0.53	10.0	0.00438	0.00265	6.03	0.00073	0.00044
Soil #2 over #1	0.69	11.8	0.02270	0.01190	17.78	0.00127	0.00067
Soil #2 over #1	0.90	12.8	0.05110	0.03050	30.45	0.00168	0.00100

Table 15
Calculated total sand flux Q, horizontal PM_{10} flux F_H, and ratio of F_H to the total mass flux q_{tot} for the Dirty Socks Sand (South Soils) from the wind-tunnel measurements

Desig.	u_* ($m\,s^{-1}$)	U_{ref} ($m\,s^{-1}$)	F_H (PM_{10}) ($g\,m^{-1}\,s^{-1}$)	F_a (PM_{10}) ($g\,m^{-2}\,s^{-1}$)	Q ($g\,m^{-1}\,s^{-1}$)	F_H/q_{tot}	F_a/q_{tot} (m^{-1})
Soil #3	0.56	9.9	0.00011	0.00004	0.47	0.00023	0.00007
Soil #3	0.67	11.2	0.00710	0.00200	23.27	0.00031	0.00009
Soil #3	0.68	11.5	0.00840	0.00288	30.94	0.00027	0.00009
Soil #3	0.75	11.4	0.00340	0.00086	16.15	0.00021	0.00005
Soil #3	0.79	12.9	0.01170	0.00319	42.03	0.00028	0.00008
Soil #3	0.84	12.6	0.01130	0.00389	39.76	0.00028	0.00010
Soil #3	1.01	12.5	0.01600	0.00709	41.35	0.00039	0.00017
Soil #3	1.02	13.0	0.01320	0.00529	39.00	0.00034	0.00014
Soil #3	1.09	13.6	0.01630	0.00692	52.38	0.00031	0.00013

Table 16
Calculated total sand flux Q, horizontal PM_{10} flux F_H, and ratio of F_H to the total mass flux q_{tot} for the UCD Fence Soil (South Soil) from the wind-tunnel measurements

Desig.	u_* ($m\,s^{-1}$)	U_{ref} ($m\,s^{-1}$)	F_H (PM_{10}) ($g\,m^{-1}\,s^{-1}$)	F_a (PM_{10}) ($g\,m^{-2}\,s^{-1}$)	Q ($g\,m^{-1}\,s^{-1}$)	F_H/q_{tot}	F_a/q_{tot} (m^{-1})
Soil #4	0.51	8.9	0.00009	0.00002	0.15	0.00057	0.00015
Soil #4	0.67	11.7	0.00220	0.00128	3.30	0.00066	0.00039
Soil #4	0.69	11.6	0.01590	0.00849	7.23	0.00220	0.00117
Soil #4	0.75	12.7	0.04150	0.02150	18.43	0.00225	0.00116
Soil #4	0.86	13.9	0.06020	0.02200	27.33	0.00220	0.00081
Soil #4	0.90	13.8	0.04320	0.02200	19.83	0.00217	0.00111

Table 17
Calculated total sand flux Q, horizontal PM_{10} flux F_H, and ratio of F_H to the total mass flux q_{tot} for the enhanced saltation of south soils from the wind-tunnel measurements

Desig.	u_* ($m\,s^{-1}$)	U_{ref} ($m\,s^{-1}$)	F_H (PM_{10}) ($g\,m^{-1}\,s^{-1}$)	F_a (PM_{10}) ($g\,m^{-2}\,s^{-1}$)	Q ($g\,m^{-1}\,s^{-1}$)	F_H/q_{tot}	F_a/q_{tot} (m^{-1})
Soil #3 over # 4	0.40	9.3	0.00010	0.00013	0.15	0.00065	0.00082
Soil #3 over # 4	0.61	11.1	0.00715	0.00199	8.68	0.00082	0.00023
Soil #3 over # 4	0.71	12.8	0.01970	0.00730	21.32	0.00093	0.00034
Soil #3 over # 4	0.75	12.9	0.01950	0.00831	21.59	0.00090	0.00039

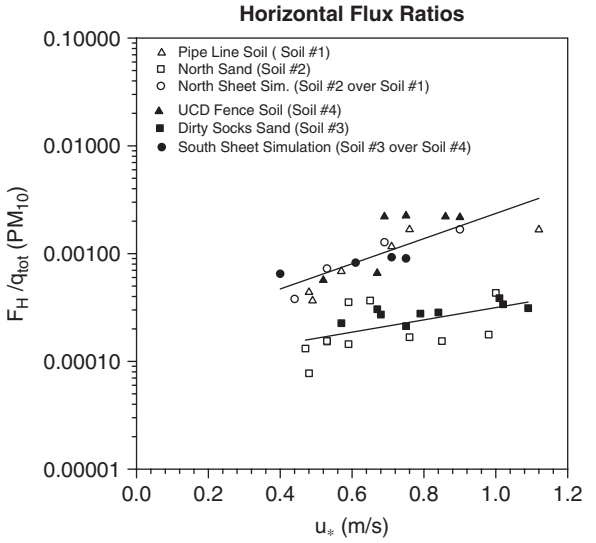

Fig. 13. PM_{10} flux to total flux ratios from the wind-tunnel experiments. Horizontal PM_{10} flux becomes a larger ratio of the total mass suspended as the friction velocity increases. High energy impacts of saltating particles are likely play the role of abrading and breaking agglomerates. There is also significant difference between sand and the emissive soils represented by the two trend lines.

were used to obtain a vertical flux ratio. At this point it is important to refer to the results presented for Owens (dry) Lake by Gillette et al. (1997a) and Niemeyer et al. (1999). Their plot (presented in both papers) specifically shows the vertical flux to total flux for seven Owens (dry) Lake cases as well as for several Western Texas agricultural soils (a compilation of many years of research). The wind-tunnel results compare favorably with the field techniques of Niemeyer et al. (1999) (sun photometer) and Gillette et al. (1997a) (multiple on-lake monitoring sites) as shown in Fig. 14. The ratios are on the same order of magnitude for the south lake location. The wind-tunnel tests designated as "UCD Fence Soil", "South Sheet Simulation" and "Dirty Socks Sand" correspond to the "Owens SW" field locations. Likewise, the other wind-tunnel cases can be compared to Gillette's Texas soils; the "North Sand" corresponding to the "sand" cases and the "North Sheet Simulation" corresponding to the "Loamy Sand" case. The ratios are similar in magnitude and behavior for the same soil types. The values of the Total Sand Flux Q, Horizontal PM_{10} Flux F_H, and Vertical PM_{10} Flux F_a are given in Tables 12–17.

4. Conclusions

The Saltation Wind Tunnel (SWT) at the University of California at Davis was employed to perform a series of experiments aimed at establishing a methodology for determining fugitive dust emission rates. As a case study, this methodology was used for quantifying the conditions for high emissions from Owens (dry) Lake soils. Four soils

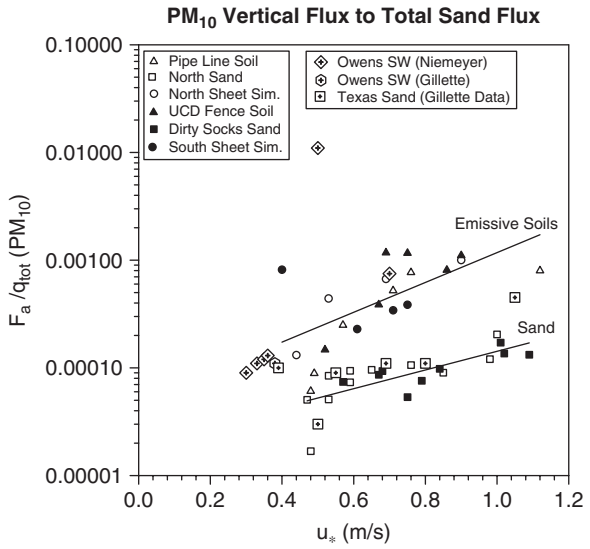

Fig. 14. Vertical PM_{10} flux to total flux ratios estimated from the wind-tunnel experiments are shown. Vertical PM_{10} flux becomes a larger ratio of the total mass suspended as the friction velocity increases. Two field studies at Owens (dry) Lake, Niemeyer et al., (1999) and Gillette et al., (1997a), show comparable numbers for the Owens Lake soils as well. Data for Texas sands also presented compare well with the sands at Owens Lake.

believed to be causal in the fugitive dust storms were targeted and emission rates obtained for varying surface conditions. Though the variables are numerous, the wind tunnel proved to be a significant aid in quantifying conditions for high emissions. First order conditions (wind, surface roughness, and soil types) similar to those at Owens (dry) Lake were matched and emission rates established for each of the four soils.

A ratio of horizontal PM_{10} flux F_H to the total soil flux q_{tot} (sand and dust) was calculated and plotted for all the cases. The wind-tunnel results for this ratio as well as the vertical flux ratio compare favorably with the field techniques of Niemeyer et al. (1999) (sun photometer) and Gillette et al. (1997a) (multiple on-lake monitoring sites) at Owens (dry) Lake. The wind tunnel, thus, provides comparable data to two separate field techniques and can be applied systematically without relying on the variability of the wind, making this technique invaluable in assessing the potential emissions of fugitive dusts.

Lastly, fetch effect studies were conducted to observe the development of emissions along the test bed. In all cases, for the soils without upwind saltation, the emissions reached an equilibrium between 2.65 and 4.38 m for the higher velocities tested. A suggested mechanism is that at the near surface, the air has become saturated and emissions are suppressed at the surface even though there is still upward entrainment of existing particles. When upwind "sand" saltation is introduced, the saturation condition disappears as the vertical flux is active due to ballistic sand impacts enhancing the dynamics of the near surface of the soil. Sand saltation again plays a dynamic role in enhancing emissions. The equilibrium condition is thus primarily the result of near surface characteristics of the soil in which severe loading near the surface prevents the same increases in emissions seen earlier in the fetch. The height limitation of the wind tunnel can also aid in reaching this saturation. The fetch effect is critical in estimating emissions at Owens (dry) Lake as well. This study shows that it is unlikely that PM_{10} emissions rate will continually increase across an erodible surface, but may instead reach saturation states. This is contrary to the Owen effect as described in Gillette et al. (1997b), which states that the horizontal mass flux or saltation should increase over the fetch, and as a result the dust emissions should also increase. However, in Gillette et al. (1997a), an increasing measured saltation rate was measured along a 100 m fetch at Owens (dry) Lake, but dust emissions decreased in the first 50 m before recovering. Thus, the wind-tunnel experiments may be exposing a near-surface saturation effect that may also occur on the playa as well.

Acknowledgments

The California Air Resources Board (CARB) funded parts of this research under the Interagency Agreement 97-718. In addition, the Great Basin Unified Air Pollution Control District (GBUAPCD) was supportive of this research effort and granted access to Owens (dry) Lake.

References

Bagnold, R.A., 1941. The Physics of Blown Sand and Desert Dunes. Chapman & Hall, Ltd., London.

Braaten, D.A., Shaw, R.H., Paw, U.K.T., 1993. Boundary-layer flow structure associated with particle reentrainment. Boundary-Layer Meteorology 65, 255–272.

Borrmann, S., Jaenicke, R., 1987. Wind tunnel experiments on the resuspension of sub-micrometer particles from a sand surface. Atmospheric Environment 21 (9), 1891–1898.

Cahill, T.A., Gill, T.E., Reid, J.S., Gearheart, E.A., Gillette, D.A., 1996. Saltating particles, playa crusts and dust aerosols at Owens (Dry) Lake, California. Earth Surface Processes and Landforms 21, 621–639.

Chepil, W.S., 1945. Dynamics of wind erosion: I. Nature of movement of soil by wind. Soil Science 60, 305–320.

Cowherd, C., Ono, D.M., 1990. Design and testing of a reduced-scale wind tunnel for surface erodibility determinations. 83rd Annual Meeting and Exhibition, Air and Waste Management Association, Pittburgh, PA, June 24–29.

Fairchild, C.I., Tillery, M.I., 1982. Wind tunnel measurements of the resuspension of ideal particles. Atmospheric Environment 16 (2), 229–238.

Gillette, D., Goodwin, P., 1974. Microscale transport of sand-sized soil aggregrates eroded by wind. Journal of Geophysical Research 79, 4080–4084.

Gillette, D.A., Walker, T.L., 1977. Characteristics of airborne particles produced by wind erosion of sandy soil, high plains of West Texas. Soil Science 123, 79–110.

Gillette, D.A., Blifford, D.A., Fenster, C.R., 1972. Measurement of aerosol size distributions and vertical fluxes of aerosols on land subject to wind erosion. Journal of Applied Meteorology 11, 977–987.

Gillette, D.A., Herbert, G., Stockton, P.H., Owen, P.R., 1996. Causes of the fetch effect in wind erosion. Earth Surface Processes and Landforms 21, 641–659.

Gillette, D.A., Fryrear, D.W., Gill, T.E., Cahill, T.A., Gearhart, E.A., 1997a. Relation of vertical flux of particles smaller than 10 μm to total aeolian horizontal mass flux at Owens Lake. Journal of Geophysical Research—Atmospheres 102 (D22), 26009–26015.

Gillette, D.A., Hardebeck, E., Parker, J., 1997b. Large-scale variability of wind erosion mass flux rate at Owens Lake 2. Role of roughness change, particle limitation, change of threshold friction velocity and the owen effect. Journal of Geophysical Research—Atmospheres 102 (D22), 25989–25998.

Kim, D., Cho, G.H., White, B.R., 2000. A wind-tunnel study of atmospheric boundary-layer flow over vegetated surfaces to suppress PM_{10} emission on Owens (dry) Lake. Boundary-Layer Meteorology 97, 309–329.

Lancaster, N., Nickling, W.G., 1994. Aeolian Sediment Transport, in Geomorphology of Desert Environments. Chapman & Hall, London.

Niemeyer, T.C., Gillette, D.A., Deluisi, J.J., Kim, Y.J., Niemeyer, W.F., Ley, T., Gill, T.E., Ono, D., 1999. Optical depth, and flux of dust from Owens Lake, California. Earth Surface Processes and Landforms 24, 463–479.

Ono, D.M., Hardebeck, E., Parker, J., Cox, B.G., 2000. Systematic biases in measured PM10 values with US environmental protection agency-approved samplers at Owens Lake, California. Journal.of Air & Waste Management. Association. 50, 1144–1156.

Pye, K., 1987. Aeolian Dust and Dust Deposits. Academic Press, London.

Roney, J.A., White, B.R., 2004. Definition and measurement of dust aeolian thresholds. Journal of Geophysical Research, Earth Surface 109, F01013.

Shao, Y., Raupach, M.R., Findlater, P.A., 1993. Effect of saltation bombardment on the entrainment of dust by wind. Journal of Geophysical Research 98 (D7), 12719–12726.

Stetler, L.D., Saxton, K.E., 1996. Wind erosion and PM10 emissions from agricultural fields on the Columbia Plateau. Earth Surface Processes and Landforms 21, 673–685.

White, B.R., 1982. Two-phase measurements of saltating turbulent boundary layer flow. International Journal of Multiphase Flow 5, 459–472.

White, B.R., Cho, G.H., 1994. Wind-tunnel simulation of the Owens Lake Sand Fences. Report, University of California, Davis, CA, prepared for Great Basin Unified Air Pollution Control District, California Air Resources Board, and the Land Commission of the State of California.

White, B.R., Roney, J., 2000. Simulation and analysis of factors leading to high PM_{10} emission fluxes at Owens (dry) Lake using and environmental wind tunnel, report, University of California, Davis, CA, prepared for the California Air Resource Board.